

Tula orthohantavirus nucleocapsid protein is cleaved in infected cells and may sequester activated caspase-3 during persistent infection to suppress apoptosis

Katherine Davies¹, Babak Afrough², Jamel Mankouri^{1,3}, Roger Hewson², Thomas A. Edwards^{1,3} and John N. Barr^{1,3}

Affiliations:

1. School of Molecular and Cellular Biology, University of Leeds, Leeds, LS2 9JT, UK
2. National Infection Service, Public Health England, Porton Down, Salisbury, SP4 0JG, UK
3. Astbury Centre for Structural Molecular Biology, University of Leeds, Leeds, LS2 9JT, UK.

Abstract: The family Hantaviridae mostly comprises rodent-borne segmented negative-sense RNA viruses, many of which are capable of causing devastating disease in humans. In contrast, hantavirus infection of rodent hosts results in a persistent and inapparent infection through their ability to evade immune detection and inhibit apoptosis. In this study, we used Tula hantavirus (TULV) to investigate the interplay between viral and host apoptotic responses during early, peak and persistent phases of virus infection in cell culture. Examination of early-phase TULV infection revealed that infected cells were refractory to apoptosis, as evidenced by the complete lack of cleaved caspase-3 (casp-3C) staining, whereas in non-infected bystander cells casp-3C was highly abundant. Interestingly, at later time points, casp-3C was abundant in infected cells, but the cells remained viable and able to continue shedding infectious virus, and together these observations were suggestive of a TULV-associated apoptotic block. To investigate this block, we viewed TULV-infected cells using laser scanning confocal and wide-field deconvolution microscopy, which revealed that TULV nucleocapsid protein (NP) colocalized with, and sequestered, casp-3C within cytoplasmic ultrastructures. Consistent with casp-3C colocalization, we showed for the first time that TULV NP was cleaved in cells and that TULV NP and casp-3C could be co-immunoprecipitated, suggesting that this interaction was stable and thus unlikely to be solely confined to NP binding as a substrate to the casp-3C active site. To account for these findings, we propose a novel mechanism by which TULV NP inhibits apoptosis by spatially sequestering casp-3C from its downstream apoptotic targets within the cytosol.

Introduction: The genus Orthohantavirus within the family Hantaviridae comprises many zoonotic segmented negative-sense RNA viruses that are capable of causing devastating human disease, often with fatal outcomes. Orthohantaviruses are broadly spherical enveloped viruses, which possess a tripartite genome made up of small (S), medium (M) and large (L) RNA segments that minimally encode the nucleocapsid protein (NP), glycoprotein precursor (GPC) and RNA-dependent RNA

polymerase (RdRp), respectively [1, 2]. Many members of the family also encode a small non-structural protein (NSs) that is accessed from an alternative open reading frame (ORF) and acts as an antagonist of the innate immune response [3–5].

Orthohantaviruses can be divided into New World (NW) and Old World (OW) clades based on their country of isolation, with OW viruses being widespread throughout Asia and Europe, and NW viruses being found in the Americas [6]. Orthohantaviruses are typically associated with a specific rodent host, although recent evidence suggests that bats, shrews, moles and ray-finned fish also act as reservoirs [7, 8]. Orthohantaviruses have been shown to cause persistent, often apathogenic infections in these hosts, although there is some evidence to suggest that infection is associated with reduced host survival [9–13], with histological examination of the lungs, heart and livers of infected animals showing some signs of pathology [14].

Orthohantaviruses are transmitted to humans by the inhalation of aerosolized excreta and other body fluids from the infected animal host, although direct human-to-human transmission has also been reported for Andes virus (ANDV) [15]. Several human pathologies have been observed for different orthohantavirus species, with the disease outcome correlating closely with the two orthohantavirus clades; OW orthohantaviruses are associated with haemorrhagic fever with renal syndrome (HFRS), whilst NW orthohantaviruses are the causative agent of hantavirus cardiopulmonary syndrome (HCPS). While these syndromes afflict different primary organs, both are characterized by excessive vascular leakage leading to shock, with human mortality rates ranging from 0.1–10 % for HFRS and up to 40 % for HCPS [16, 17]. Endothelial cells are the primary sites of hantavirus multiplication, although these cells do not display overt cytopathic effects [18]. This outcome is recapitulated in cell culture systems in which orthohantavirus infections are not associated with excessive cytopathology or cell lysis, and instead infections can become persistent with ongoing virus shedding for up to 139 days post-infection in the case of Seoul virus (SEOV) [19–21]. The ability of hantaviruses to persist suggests that they are able to evade pathogen surveillance, and avoid innate immune defence mechanisms such as apoptosis.

Apoptosis is an important component of cellular homeostasis. There are many apoptotic pathways, including the caspase cascade, in which a series of cysteine–aspartate proteases are activated by cleavage [22]. Viruses have developed complex mechanisms to modulate apoptotic signalling pathways to benefit their own survival, which can result in either delay or acceleration of apoptosis with pro-viral outcomes.

There is considerable evidence to suggest that hantaviruses prevent the induction of apoptosis, which is consistent with their ability to establish persistence. Puumala virus (PUUV) NP has been shown to interact with the Fas-mediated apoptosis enhancer Daxx [23], whilst NP from Hantaan virus (HTNV)

modulates apoptosis by down-regulating p53 [24]. Furthermore, a panel of six hantaviruses spanning three distinct serogroups [ANDV, Dobrava virus (DOBV), HTNV, PUUV, SEOV and Tula virus (TULV)] were each recently shown to suppress apoptosis in staurosporine-treated cells. The same study suggested that NP plays a direct role in modulating apoptosis through the demonstration that NP can be cleaved by purified caspase-3. In addition, recombinant N protein from ANDV, DOBV and PUUV have been shown to inhibit both caspase-3 and granzyme B in cell-free assays [25, 26].

To better characterize the role of the hantavirus NP in modulating apoptosis, we used the model OW orthohantavirus TULV to examine how NP interacts with key components of the apoptotic machinery through an extended time course spanning early infection, peak infection and a persistently infected state. We demonstrate that TULV infection can persist for over 30 days in mammalian cells, with little or no apoptosis induction despite abundant levels of cleaved caspase-3 (casp-3C). We further show that TULV NP forms both punctate and tubular ultrastructures within intermediate and persistently infected cells, in which active casp-3C is physically sequestered as a consequence of a robust and stable association with NP, leading to NP cleavage. We thus propose a model in which the ability of TULV to suppress apoptosis is driven by interactions between NP and casp-3C, leading to NP cleavage and spatial separation of the executioner caspase from its downstream effectors.

Results

Generation of tools to quantify TULV components and infectivity: To characterize the progression of TULV infection in cells throughout an extended time course, we first developed tools to accurately quantify both TULV components and infectivity. For TULV protein detection, we generated NP antisera, and based on phylogenetic analysis of OW clade hantavirus NP amino acid sequences, we selected the SEOV NP to raise polyclonal antisera that would be broadly cross-reactive to multiple hantavirus NPs, including TULV. The SEOV NP core (residues 111–399; NPcore) was bacterially expressed and purified (Fig. 2a, left panel) and used for antibody production. The resulting antisera showed cross-reactivity against recombinant SEOV NPcore expressed in bacteria by Western blot analysis (Fig. 2a, right panel) and against TULV NP generated in TULV-infected cells at 6 days p.i., as assessed by both Western blotting (Fig. 2b) and immunofluorescence (Fig. 2c). These results confirmed the high specificity of the antisera, as evidenced by absent background or non-specific staining in mock-infected cells. In agreement with previous studies, TULV NP was detected in perinuclear ultrastructures and cytoplasmic puncta [20]. Alongside the production of NP antisera, we also established a rapid PCR-based assay for the quantitative detection of TULV vRNA replication products, calibrated using a standard curve generated using *in vitro*-transcribed TULV S segment vRNA at a range of concentrations. The purity of the vRNA was verified using electrophoresis (Fig. 2d) and Rsq values

≥ 0.99 (Fig. 2e). Finally, we developed assays to measure TULV infection kinetics and virus production. Conventional infectivity assays that are reliant on plaque formation are problematical due to the low cytopathology of hantaviruses, with hantavirus infectivity often being measured by neutral red uptake, which is both time-consuming and inaccurate, taking 10 days to produce poorly visible plaques (Fig. 1a). To remedy this, we developed an immunofluorescence (IF)-based assay that relies on TULV NP antisera for the detection of infected cells (Fig. 1b). This method was used to examine the infectivity of a TULV dilution series and the infected cell numbers followed a linear curve with a R_{sq} values ≥ 0.99 (Fig. 1c).

Quantification of TULV components and infectivity across a 30-day time course: We next examined TULV multiplication and infectious particle production in Vero E6 cells over an extended time course. Cells were infected at an m.o.i. of 0.1, after which supernatants and cell lysates were collected at regular time points up to 10 days p.i., with infections carried out at both 32 and 37 °C. Additional samples from cultures incubated at 37 °C were also taken at 15, 20, 25 and 30 days p.i. NP antisera was used to measure NP accumulation in cell lysates harvested from 37 °C cultures by Western blotting, which served as a marker for viral gene expression and virus growth. Amplification of intracellular NP was first detected at 1 day p.i. (Fig. 3a; 24 h p.i.), indicating a significant lag prior to the onset of detectable gene expression, and also reflecting the low m.o.i. used. Following this, NP abundance increased until 3 days p.i. (Fig. 3a; 72 h p.i.), at which time NP abundance reached a plateau that did not decline up to 10 days p.i. (Fig. 3a; 240 h p.i.). NP abundance relative to GAPDH was calculated using densitometry and represented graphically alongside (Fig. 3a).

Concomitantly, we used qRT-PCR to quantify the abundance of viral S segment RNAs, harvested as virion-associated RNA within released virus particles in the supernatant. This revealed a complex pattern that comprised an initial lag phase up to 30 h p.i., where viral RNA levels showed no increase over input, indicating an initial lag in genome production and virus release. This was subsequently followed by an exponential phase of rapid genome production, and a plateau in RNA detection that extended to 10 days p.i. This pattern of RNA detection was observed in TULV grown at both 32 and 37 °C (Fig. 3b) and was consistent with the profile of NP detection shown above (Fig. 3a). At later time points (15–30 days p.i.) genome abundance did not increase further and gradually declined until the final 30 days p.i. measurement, although the vRNA abundance remained at least 1 log higher than the initial input (Fig. 3c).

To confirm that the detected RNA levels were due to the release of infectious virus particles, and not the release of defective or fragmented RNAs, we also measured TULV infectivity in the supernatants (Fig. 3d , e). The overall pattern of infectivity closely followed that of genome RNA abundance, with the release of infectious virus remaining at a consistent level until the harvest at 30 days p.i., a

hallmark of a persistent infection. Based on these observations, we defined 1.5, 7 and 30 days p.i. as the time points representing distinct early, peak and persistent phases of virus multiplication, respectively.

In fact, analysis of TULV-infected cultures using NP antisera at 1.5, 7 and 30 days p.i. time points correlated with the above metrics (Fig. 3f). At 1.5 days p.i., NP staining was punctate and perinuclear, whereas at 7 and 30 days p.i., the staining pattern changed noticeably, with NP forming tubular ultrastructures in addition to distinct puncta. There was little evidence of nuclear fragmentation in infected cells at any of these time points, which was suggestive of a lack of virus-induced apoptosis, although multinucleate syncytia were observed in the 30 days p.i. cultures.

TULV infection interferes with apoptotic induction in Vero E6 cells: The results thus far showed that cultures of TULV-infected Vero E6 cells can be maintained for up to 30 days p.i. without major cytopathic effects. This suggests that TULV infection does not readily lead to cell death, correlating with previous work that demonstrated the ability of hantaviruses to subvert apoptotic induction. To further examine the apoptotic response of Vero E6 cells to TULV infection, infected cell lysates were collected every 24 h up to 10 days p.i., and again at 30 days p.i., and the levels of total caspase-3, cleaved caspase-3 (casp-3C) and cleaved poly (ADP-ribose) polymerase (PARP-C) were assessed (Fig. 4).

Total caspase-3 was detected in TULV-infected cells, with its abundance increasing at later time points due to cell proliferation, which is consistent with the increasing abundance of the GAPDH loading control. The activated derivative casp-3C, which is indicative of apoptosis induction, was detected in TULV cell lysates from 5 to 6 days p.i., with its abundance increasing up to 10 and 30 days p.i. However, whilst this was suggestive of TULV-induced apoptosis in infected cell cultures, a lack of PARP-C was evident at 6–10 days p.i., and only moderate PARP-C cleavage was observed at 30 days p.i. Furthermore, the high levels of casp-3C at 30 days p.i. were inconsistent with the apparent health of cells in these persistent cultures (Fig. 3f). Taken together, these findings suggest that although the executioner casp-3C was present in its active form, it failed to trigger cell death in TULV-infected cells, possibly due to the activity of a TULV component.

TULV induces apoptosis in bystander cells: The results thus far suggested that the downstream activity of executioner casp-3C may be suppressed in TULV-infected cells. We therefore investigated the intracellular location of casp-3C in relation to TULV NP in individual cells, first at 1.5 days p.i., which is representative of the early stages of infection.

At 1.5 days p.i., ~10 % of cells were infected, as evidenced by characteristic punctate TULV NP staining, with the numbers of infected cells correlating with the initial m.o.i. of 0.1 (Fig. 5a). In TULV-infected cells, NP staining was abundant, whilst minimal casp-3C was detected. Interestingly, casp-3C was

abundant in uninfected bystander cells (four examples are shown in Fig. 5b), with casp-3C staining in a punctate distribution that extended throughout the cytoplasm, suggesting apoptotic induction, possibly through receiving indirect pathogen recognition signals from adjacent TULV-infected cells. We propose that the likely fate of these cells is death. Casp-3C staining was detected in over 60 % of bystander cells, but only in 4 % of TULV-infected cells (Fig. 5c). Fluorescent line scan analysis (Fig. 5b, right panel) quantified the expression of casp-3C in one such bystander cell, and revealed clear segregation from the TULV N stain in an adjacent infected cell (Fig. 5d). These data suggest that during the early stages of virus infection, TULV is not a potent inducer of apoptosis, most likely because of the ability of a TULV component to suppress apoptotic stimuli.

TULV NP sequesters casp-3C at later stages of infection: At 7 days p.i., the majority of cells were infected by TULV, as evidenced by the accumulation of NP, which exhibited both punctate staining and the formation of large tubular perinuclear structures (Fig. 3f and (Fig. 6a). These TULV infected cells exhibited casp-3C staining, but it was noticeable that the levels of staining in relation to that exhibited within non-infected bystander cells was low, consistent with the suppression of apoptosis by a TULV component. Interestingly, quantification of TULV NP and casp-3C staining by fluorescent line scan analysis revealed several instances of colocalization between the two markers within both characteristic puncta and larger tubular structures (Fig. 6a, zoomed merge panel and associated line scan, left), although in other areas, the two signals were separate.

Examination of TULV persistently infected cultures at 30 days p.i. revealed all cells to be TULV-infected, and exhibiting characteristic TULV NP staining within both discrete puncta and larger tubular structures. As at 7 days p.i. (Fig. 6a), casp-3C was detected in these TULV-infected cells and fluorescent line scan analysis (Fig. 6b, zoomed merge panel and associated line scan, left) revealed the colocalization of casp-3C with NP in both punctate and large tubular structures.

At these peak and persistent time points (7 and 30 days p.i.), when casp-3C was detected in TULV-infected cells, a distinct lack of apoptosis within the cells was evident, with most cells apparently healthy and able to sustain virus production (Fig. 3e). These observations were difficult to reconcile with the abundance of casp-3C observed in these cells, other than through a scenario in which active casp-3C was prevented from cleaving downstream substrates in the caspase cascade, possibly through its interaction with TULV NP.

Examination of TULV NP and casp-3C colocalization using wide-field deconvolution microscopy (WFDM): To further examine the colocalization of TULV NP and casp-3C in persistently infected cells at 30 days p.i., infected cells were assessed by WFDM to enhance the detection sensitivity. As with confocal microscopy (Fig. 6), WFDM revealed that TULV-infected cells exhibited casp-3C staining within discrete cytoplasmic puncta (Fig. 7a). While some areas of casp-3C staining were distinct from

TULV NP, a high level of colocalization was observed, with the casp-3C staining appearing to be contained within that of TULV NP. Analysis of the spatial distribution of the two proteins using multiple fluorescent line scan analyses (Fig. 7b, line scans below) confirmed and quantified the TULV NP and casp-3C colocalized signals, consistent with a scenario in which TULV NP compartmentalizes casp-3C. Quantification of TULV NP/ casp-3C puncta abundance across early, peak and persistent TULV cultures revealed an increased number of colocalized puncta through progression of the 30-day time course, with nearly 30 % colocalization of the two proteins at 30 days p.i. (Fig. 7b, histogram). In other areas of persistently infected cells, NP and casp-3C staining remained separate, and were quantified using multiple line scans (Fig. 7c), with the quantitation of colocalization in early, peak and persistent TULV cultures being represented as a histogram.

TULV NP is cleaved in infected cells and associates robustly with casp-3C: For the orthohantavirus members ANDV, DOBV and PUUV, recombinant casp-3C has been shown to mediate cleavage of their respective purified NPs in cell-free assays [26]. In the case of ANDV, casp-3C cleaves ANDV NP at the sequence DLID285, which conforms to the consensus DXXD motif for caspase-3 cleavage and generates a major NP fragment with a molecular mass of approximately 35 kDa. With this knowledge, combined with our observation that casp-3C and NP colocalize in TULV-infected cells, we next explored the possibility that TULV-NP acted as a cleavage substrate in infected cells.

Analysis of the TULV NP sequence revealed the presence of an identical DLID motif that is found in the ANDV NP, which was previously shown to be recognized and cleaved by casp-3C in cell-free assays. Interestingly, whilst the DLID motif was present in NPs from ANDV and TULV, it was absent in HTNV, PHV and SEOV (Fig. 8a). Cleavage of the TULV NP at this site was predicted to generate TULV NP fragments of ~32 and ~16 kDa. To test whether cleavage at this site occurs during infection, we examined TULV-infected cell lysates for NP-derived cleavage products by Western blotting using anti-NP antisera, which revealed the abundant presence of NP cleavage products precisely matching these predicted masses (NP 32 and NP 16 kDa, respectively; Fig. 8b). The 16 kDa NP fragment was detected with high abundance at 3 days p.i., which coincided with the initial detection of full-length NP, suggesting that NP cleavage occurs early during TULV infection. The fact that TULV NP possesses the same casp-3C target motif as ANDV, along with the consistent colocalization of TULV NP and casp-3C shown above, strongly implicates casp-3C as being responsible for the TULV NP cleavage we observed. To further examine the TULV NP and casp-3C interaction, we next performed co-immunoprecipitation analysis using TULV NP antisera to pull down TULV NP and its interacting partners from 30 days p.i. TULV-infected cells. Subsequent Western blot analysis of eluted fractions revealed the presence of full-length NP, as well as cleaved NP 32 and NP 16 kDa forms, along with abundant casp-3C (Fig. 8c). These data are entirely consistent with the co-localization studies described above (Fig. 7b) and show

that the TULV NP and casp-3C interaction is highly stable. The ability of NP to pull down casp-3C with such abundance argues for a scenario in which the interaction involves residues that are not confined to the casp-3C active site, which alone would be expected to result in an extremely transient enzyme : substrate interaction that would not be amenable to immunoprecipitation.

Taken together, we demonstrate for the first time that a hantaviral NP interacts with casp-3C in infected cells in a robust and stable manner, and we suggest that the nature of this interaction results in physical sequestration of casp-3C within NP compartments, and drives the suppression of the apoptotic response.

Discussion: Here, we investigated the interplay between TULV and apoptosis induction in Vero E6 cells throughout an extended time course, spanning early, peak and persistent phases of infection. Previous work [23, 25, 26, 29] has shown that TULV and other hantaviruses inhibit apoptosis, and two observations made in our current study lend support to this proposal. First, while casp-3C was undetectable in TULV-infected cells at 1.5 days p.i., in the same cultures, casp-3C was highly abundant in non-infected bystander cells, consistent with the ability of a TULV component to block apoptotic induction. Second, we showed that TULV can form persistently infected cultures up to 30 days p.i. without significant levels of cytopathic effects or the development of an apoptotic phenotype, despite casp-3C being highly abundant.

Our finding that TULV hinders apoptotic induction is in agreement with published work, but is in conflict with some previous studies in which TULV infection was associated with abundant detection of apoptotic markers by Western blotting [30–32]. However, we propose that this discrepancy may have arisen through technical differences in the approaches used to detect apoptotic markers. Here, we examined the spatial distribution of both NP and apoptotic markers in individual cells, rather than culture lysates that comprise both infected and uninfected cells. Whilst fluorescent imaging resulted in the abundant detection of casp-3C at early time points following infection, it was predominantly located in bystander cells, rather than in TULV-infected cells. Thus, we propose that apoptosis of bystander cells, rather than TULV-infected cells, may be the source of the apoptotic markers observed in previous studies. Bystander effects have been described previously in SEOV, HTNV, ANDV [31] and HIV, where the Env glycoprotein induces apoptotic induction in neighbouring cells [33], and have been utilized in cancer therapy by employing ‘suicide genes’ that allow the production of a toxic metabolite that acts deleteriously on neighbouring cells [34].

Previous work has shown that a variety of hantaviral NPs, either expressed recombinantly or purified from virions, can be cleaved in cell-free assays by recombinant activated caspase-3. Here, we show that TULV NP is cleaved during infection (Fig. 8a), with the apparent mass of released fragments being consistent with caspase-3 cleavage at a conserved DLID sequence, identical to that recently identified

as a caspase-3 cleavage site for ANDV NP [26]. The role of TULV NP cleavage in these infected cells remains undetermined. One possibility is that it acts as a 'decoy' substrate, as was reported for Junin arenavirus (JUNV) [35], in which the JUNV NP delays the onset of apoptosis by acting as a 'caspase sink', diverting caspase-3 from the cleavage of downstream effectors. An equivalent scenario for TULV NP is entirely consistent with our findings that TULV NP associates with casp-3C and is cleaved, as well as the established ability of TULV to delay the apoptotic response.

However, we suggest that NP might delay or hinder the apoptotic response using a different mechanism. The ability of NP to interact with casp-3C, as determined by both indirect immunofluorescent imaging and immunoprecipitation analysis, reveals a highly robust interaction. Interestingly, line scans (Fig. 7b) revealed that the TULV NP and casp-3C colocalizing signals did not occupy precisely the same positions, rather NP appeared to form a distinct boundary around casp-3C, suggestive of a virus-induced compartment in which casp-3C was physically separated from the cytosolic environment. The demonstration that casp-3C and NP could be immunoprecipitated by NP antisera is perhaps not surprising given the extensive immunofluorescent colocalization described above, but it reveals a robust and stable casp-3C/NP interaction, and one that differs from a canonical enzyme : substrate interaction that involves binding at the active site alone. The apparent stability of the TULV NP and casp-3C interaction, as demonstrated by their co-immunoprecipitation, argues that the interaction likely encompasses additional residues outside of the active site, and that the association of these two components is not transient.

Based on this evidence, we propose a model in which TULV NP compartmentalizes casp-3C and physically separates it from downstream components of the caspase apoptotic cascade. This mechanism of apoptosis protection has previously been demonstrated in other types of human disease. In Alzheimer's disease, amyloid- β ($A\beta$) fibrils sequester caspase-3 into compartments to protect cells from apoptosis [36]. Heat shock protein 27 (Hsp27) also sequesters procaspase-3 and cytochrome-c, which prevents the formation of the apoptosome during thermotolerance [37]. In addition, the ced-9 molecule, a Bcl-2 homologue that is found in *Caenorhabditis elegans*, is a well-established example of a protein that regulates apoptosis by sequestering the caspase activating factor ced-4, an analogue of mammalian Apaf-1, to the mitochondria, preventing non-programmed apoptosis. When the interaction between ced-9 and ced-4 is disrupted, downstream caspase cleavage and subsequent activation result in apoptosis [38–40]. These examples provide precedents for apoptotic protein sequestration acting to prevent apoptosis in both health and disease systems.

In summary, the colocalization and co-precipitation of TULV NP and casp-3C, paired with the presence of a casp-3C recognition site, provides evidence that NP is involved in interference with the host cell apoptotic pathway. We therefore suggest that TULV NP interferes with apoptosis by binding to and

sequestering active caspase-3 in NP-coated compartments, preventing casp-3C from activating its downstream substrates.

Fig. 1. TULV immunofluorescent infectivity assay. (a) An example of a neutral red plaque assay well at 10⁻³ dilution displaying typical indistinct hantavirus plaques. (b) Example images of TULV-infected or mock-infected wells used for the immunofluorescent infectivity assay using anti-NP antisera and the Incucyte ZOOM instrument, with (IF) and without (object mask) analysis using masking software to count immunofluorescent units. (c) Linear range describing the dilution factor of the immunofluorescent assay.

Fig. 2. Identification and quantification of TULV components. (a) Bacterially expressed and purified recombinant SEOV NPcore used for antigen production migrated with an apparent molecular weight of ~30 kDa following SDS-PAGE, as visualized by Coomassie staining. The SEOV NPcore was detected by Western blotting using NPcore antisera. (b) Cross-reactivity of the SEOV NPcore antisera against TULV NP (~50 kDa) expressed in infected Vero E6 cell lysates, shown by Western blotting. Cell lysates were collected at 120 h p.i. and GAPDH was used as a loading control. (c) Indirect immunofluorescence images of TULV-infected and mock-infected Vero E6 cells using the NP antisera, taken on a Zeiss LSM880 confocal microscope using 40× magnification, with the white bar representing 20 μM. Nuclei are shown in blue and TULV NP is shown in green. (d) In vitro-transcribed TULV S segment vRNA, serially diluted to form a calibration curve for quantitative RT-PCR. (e) Example calibration curve generated experimentally by quantitative RT-PCR.

Fig. 3. Kinetics of TULV replication in Vero E6 cells. (a) Western blot using anti-TULV NP and anti-GAPDH antibodies of TULV-infected Vero E6 cell lysates collected at time points spanning 1–10 days p.i., with NP levels quantified using densitometry in relation to the GAPDH loading control. (b) TULV RNA genome copies ml⁻¹ as quantified using one-step quantitative RT-PCR on samples collected 1–10 days p.i., and (c) extended to 1–30 days p.i. (d) TULV infectious titres determined by the immunofluorescence infectivity assay on samples collected 1–10 days p.i., and e) extended to 1–30 days p.i. (f) Laser scanning confocal images taken of TULV-infected Vero E6 cells at 1.5 days p.i., 7 days p.i. and 30 days p.i. using 40× magnification and stained using anti-TULV NP antisera, with the white bar representing 20 μM. Nuclei were stained with DAPI and are shown in blue and TULV NP is shown in green.

Fig. 4. Examination of the induction of apoptotic markers during TULV infection of Vero E6 cells. TULV-infected Vero E6 cell lysates collected from 1 to 10 days p.i. and 30 days p.i. and examined by Western blotting for the presence of TULV NP, pre-caspase-3 (casp-3), active caspase-3 (casp-3C) and cleaved PARP (PARP-C), alongside a GAPDH loading control.

Fig. 5. Detection of active cleaved caspase-3 in bystander cells, but not infected cells, within TULV-infected Vero E6 cultures. (a) Indirect immunofluorescence of TULV-infected Vero E6 cells at 1.5 days p.i. using antisera specific for TULV NP and cleaved caspase-3 (casp-3C). The images were taken using laser scanning confocal microscopy with 40× magnification, with casp-3C shown in red, TULV NP shown in green and DAPI shown in blue. The white bar represents 20 μM. (b) Merged zoom images of four representative bystander cells with the white bar representing 10 μM. (c). Quantification of the percentage of TULV-infected and bystander cells exhibiting casp-3C staining. (d). Fluorescent line scans of both bystander and TULV-infected cells of the right-hand merge panel shown in panel (a), taken along the grey bars using Fiji software, with the red line representing NP and the green line representing casp-3C .

Fig. 6. Active caspase-3 colocalizes with TULV NP in the cytoplasm at later stages of infection. (a) Indirect immunofluorescence of Vero E6 cells infected with TULV at 7 days p.i. or (b) 30 days p.i. Images were taken using laser scanning confocal microscopy using 100× magnification, with casp-3C signal in red, nucleocapsid protein (NP) in green and DAPI in blue, with the white bar representing 20 μM. Merged images are shown on the right, with a zoomed merge in which the white bar represents 10 μM. A fluorescent line scan was taken along the grey bar shown on the zoomed merged image using Fiji software, with the red line representing NP and the green line representing casp-3C.

Methods:

Cell culture: TULV Moravia strain 5302 v/95 and Vero E6 cells were kindly provided by Dr Roger Hewson, Public Health England, UK. Virus propagation was carried out in Vero E6 cells grown in Dulbecco's modified Eagle's medium (DMEM) supplemented with 10 % foetal bovine serum (FBS) (Sigma Aldrich), 100 U ml⁻¹ penicillin and 100 μg ml⁻¹ streptomycin at 37 °C in a 5 % CO₂ atmosphere. TULV stocks were confirmed as mycoplasma-free using MycoAlert (Lonza).

Nucleocapsid protein production and purification: A cDNA representing the NP ORF from SEOV strain Humber (accession number JX879769.1), optimized for bacterial expression, was generated synthetically (GeneArt, Thermo Fisher Scientific) and inserted into the pMK-RQ vector. This was subsequently used as the template for amplification of the NP 'core', comprising residues E111–G399 (NPcore), using the primer set 5'- TGTTGGATCCGAACCGACAGGTCAGACCGCAGATTG-3' and 5'- GGTGCTCG AGTTAACC CAGG TGAA AGTT ATCCACG GC-3'. The amplified core region was then cloned into the pET28a (+) expression vector behind sequences for both the 6xHis affinity tag and the SUMO tag for overexpression in Escherichia coli BL21 DE3 Gold cells. Bacterial cultures were induced using 0.5 mM IPTG and then incubated overnight at 18 °C in a 180 r.p.m. shaking incubator. Bacterial pellets

were collected by centrifugation at 4000 g for 20 min at 4 °C before resuspension in ice-cold lysis buffer [500 mM NaCl, 20 mM Tris-HCl pH 8, 20 mM MgCl₂, 5 mM β-mercaptoethanol, 1 % Triton X-100, 1 mg ml⁻¹ lysozyme (Sigma Aldrich), 1 pellet EDTA-free protease inhibitors (Roche), 1 U RNase, 1 U DNase) and sonicated. The insoluble fraction was pelleted by centrifugation at 20 000 g for 1 h at 4 °C and soluble protein was collected in the supernatant. The soluble fraction was then applied to a 5 ml HisTrap (GE Healthcare) column and washed with 5 column volumes of 25–100 mM imidazole wash buffers (500 mM NaCl, 20 mM Tris, 5 mM β-Me). Recombinant NPcore was eluted from the column using 10 column volumes of elution buffer (500 mM imidazole, 500 mM NaCl, 20 mM Tris, 5 mM β-mercaptoethanol). The 6xHis SUMO tag was removed by incubation with 1 U ml⁻¹ Ulp1 protease overnight at 4 °C. The cleaved protein was diluted 1 : 10 in 20 mM elution buffer before being passed over a 5 ml HisTrap column to remove tag and protease. The collected flow-through was concentrated in a 10 kDa molecular weight cut-off concentrator (Amicon) to 0.5 mg ml⁻¹. The purity (>85 %) of the resulting NPcore was determined by densitometry following SDS-PAGE and Coomassie staining.

Antibodies: TULV NP antibody was generated in sheep with 4×200 mg inoculations of recombinant purified NPcore (Alta Biosciences). Serum was collected pre-inoculation and post-one, -two, -three and -four inoculations. The serum was centrifuged at 4000 g for 20 min at 4 °C to remove debris before being stored at -20 °C. Polyclonal antibodies against cleaved caspase-3, caspase-3 and cleaved PARP were purchased from New England Biolabs and monoclonal antibodies against GAPDH were purchased from GeneTex.

Quantitative reverse transcriptase-PCR: Quantitative RT-PCR was carried out as previously described [27] with adaptations to the GoTaq 1-Step RT-qPCR system protocol (Promega). TULV S segment RNA was isolated from infected cell culture medium using a viral RNA mini kit (Qiagen) and reverse-transcribed using the primers 5'- GCCT CTAG AATG AGCC AACT CAAA GAAA TACAAGAGG-3' and 5'- GCCC TCGA GTTA GATT TTTA GCGGTTCC TGGTTTG-3'. The S segment ORF was sub-cloned into pCDNA3.1 (+) T7 expression vector and used as template for transcription S segment RNA using the mMMESSAGE mMACHINE T7 Transcription kit (Thermo Fisher Scientific) and purified using the RNeasy mini kit (Qiagen). RNA purity was assessed using electrophoresis examination (Fig. 1a) and the concentration was adjusted to 108, 106, 104 and 102 genomic copies per quantitative RT-PCR (qRT-PCR) reaction (5 μl). Genomic copies of experimental samples were determined from the generated standard curve.

Virus infections: Vero E6 cells were seeded out at a density of 1×10⁵ cells per well for a 12-well plate or 1×10⁶ cells per 25 cm² flask. TULV was adsorbed to monolayers at a multiplicity of infection (m.o.i.) of 1–0.1 in DMEM for 90 min before DMEM supplemented with 2 % FBS, 100 U ml⁻¹ penicillin and

100 $\mu\text{g ml}^{-1}$ streptomycin (2 % DMEM) was added. Persistent TULV infections were carried out in 25 cm^2 flasks and infected cells were seeded onto coverslips 24 h before fixation. Cells were fixed in 4 % paraformaldehyde at 36 h post-infection (p.i.), 7 days p.i. and 30 days p.i. to demonstrate early, peak and persistent infections.

TULV time course: Vero E6 cells were seeded out at a density of 6×10^5 cells per well of a six-well plate and infected with TULV at an m.o.i. of 0.1. At each time point, cells were scraped into the cell culture medium and stored at -80°C . Cell cultures were clarified by centrifugation at 20 000 g for 10 min at 4°C . RNA extractions were carried out on clarified cell culture supernatant using a viral RNA mini kit (Qiagen) and RNA was quantified in duplicate using one-step qRT-PCR. Infectious TULV was titrated in triplicate using an immunofluorescence assay.

Virus titration: Vero E6 cells were seeded out at a density of 5×10^3 cells per well of a 96-well plate or at 6×10^5 cells per well of a 6-well plate and incubated at 37°C in a 5 % CO_2 incubator overnight. TULV was diluted 10⁻¹ to 10⁻⁵ at a 1 : 10 dilution in DMEM. Diluted virus was adsorbed to cell monolayers alongside neat TULV in volumes of 100 μl (96-well) and 200 μl (6-well). TULV was adsorbed for 90 min at 37°C on a rocking platform. Following adsorption, 100 μl 2 % FBS DMEM was added to 96-well plate cells and incubated at 37°C for 72 h in a 5 % CO_2 incubator. For six-well plates, inoculum was removed and overlaid with 3 ml 2 % agarose diluted 1 : 1 in 2 % FBS DMEM and this was added to each well and incubated at 37°C for 7 days in a 5 % CO_2 incubator. A second overlay of 2 ml 2 % agarose diluted 1 : 1 in 2 % FBS DMEM was added containing 45.3 $\mu\text{g ml}^{-1}$ neutral red (Sigma Aldrich) before incubation at 37°C in a 5 % CO_2 incubator for a further 3 days. Plaques were considered to be areas with reduced staining and these were counted [28]. Ninety-six-well plate cells were fixed in ice-cold methanol and infected cells were identified through indirect staining using the anti-NPcore antibody in conjunction with an Alexa Fluor 488 secondary antibody (Thermo Fisher Scientific). The Incucyte Zoom instrument (Essen Bioscience) using a 10 \times objective lens was used to image infected monolayers. The Incucyte ZOOM software was used to calculate the number of infected cells per well by extrapolating an average a value from three fluorescent images of each well. Infectivity was quantified as immunofluorescent units per ml (IU ml^{-1}), which represented the number of resulting infectious foci per ml of inoculum. Each sample was quantified in triplicate.

Indirect immunofluorescence: Infected monolayers on coverslips were permeabilized in ice-cold methanol and incubated at -20°C for at least 1 h before being washed in 1 \times PBS and blocked in 5 % BSA in 1 \times PBS (produced in-house). Primary antibody staining was carried out in 1 % BSA in 1 \times PBS using sheep anti-NPcore at 1 : 2000 dilution and rabbit anti-cleaved caspase-3 (casp-3C) antibody at 1 : 200 dilution. Incubations were carried out for 2 h at room temperature, followed by thorough washing in 1 \times PBS. Secondary antibody staining was carried out using donkey anti-sheep Alexa Fluor

488 and donkey anti-rabbit Alexa Fluor 647 at a 1 : 1000 dilution for 1 h. DAPI staining was carried out by incubation with 300 mM DAPI for 5 min at room temperature. Coverslips were mounted onto slides using VECTASHIELD Antifade Mounting Medium (Vector Laboratories) and sealed using clear nail polish. Infected cells were imaged using the Zeiss LSM880 upright confocal microscope at 40× magnification (Carl Zeiss Ltd) and the DeltaVision Widefield Deconvolution microscope at 100× magnification (GE Healthcare).

Western blotting: TULV infections, as described above, were carried out on Vero E6 monolayers in six-well plates. At 24, 48, 72, 96, 120, 144, 168, 192, 216 and 240 h p.i. cells were scraped into cell culture medium and collected by centrifugation at 20 000 g for 10 min at 4 °C before resuspension in 50 µl PBS. An equal volume of NuPage loading buffer (Thermo Fisher Scientific) was added and samples were heated at 95 °C for 5 min. Protein samples were separated by 15 % SDS-PAGE and then transferred to an Immobilon-FL polyvinylidene difluoride (PVDF) membrane (Merck Millipore), which was probed with sheep anti-NPcore, rabbit anti-cleaved caspase-3 (casp-3C), caspase-3 (casp-3) and cleaved PARP (PARP-C). Mouse anti-GAPDH antibody was used as a loading control. Protein was detected using IRDye 800CW donkey anti-goat IgG (H+L), IRDye 800CW donkey anti-rabbit IgG (H+L) and IRDye 680RD donkey anti-mouse IgG (H+L), and visualized by the Odyssey Imaging system (LI-COR). Densitometry was carried out using Fiji software.

Co-immunoprecipitation: Three 175 cm³ flasks of Vero E6 cells at 60 % confluence were infected with TULV at an m.o.i. of 0.1, as previously described. At 30 days p.i. cells were scraped into the cell culture medium and centrifuged at 4000 g for 10 min at 4 °C. The supernatant was discarded and the cell pellet was washed in 1× PBS, followed by resuspension in ice-cold lysis buffer [150 mM NaCl, 50 mM TrisHCl (pH 8.0), 1 % NP-40 alternative, 0.1 % sodium dodecyl sulphate, 1× EDTA-free protease inhibitor tablets (Roche)], and incubated on ice for 30 min before being clarified by centrifugation at 1000 g for 10 min. Clarified lysate was used for TULV NP immunoprecipitation with anti-NPcore using the Dynabeads protein G immunoprecipitation kit (Thermo Fisher Scientific) following the manufacturer's instructions. Then 1× NuPAGE loading dye was added directly to the beads and the samples were heated at 95 °C for 5 min. The samples were centrifuged at 10 000 g to pellet the beads and supernatant was added to SDS-PAGE gels. Mock samples were treated similarly to infected samples, but without the addition of TULV.

References

1. Schmaljohn CS, Dalrymple JM. Analysis of Hantaan virus RNA: evidence for a new genus of Bunyaviridae. *Virology* 1983;131:482–491.

2. Schmaljohn CS, Hasty SE, Harrison SA, Dalrymple JM. Characterization of hantaan virions, the prototype virus of hemorrhagic fever with renal syndrome. *J Infect Dis* 1983;148:1005–1012.
3. Plyusnin A. Genetics of hantaviruses: implications to taxonomy. *Arch Virol* 2002;147:665–682.
4. Virtanen JO, Jääskeläinen KM, Djupsjöbacka J, Vaheri A, Plyusnin A *et al.* Tula hantavirus NSs protein accumulates in the perinuclear area in infected and transfected cells. *Arch Virol* 2010;155:117–121.
5. Matthys V, Mackow ER. Hantavirus regulation of type I interferon responses. *Adv Virol* 2012;2012:1–9.
6. Briese T, Alkhovsky SV, Beer M, Calisher CH, Charrel RN *et al.* Bunyavirales proposal. *Ictv* 2016:1–45.
7. Guo WP, Lin XD, Wang W, Tian JH, Cong ML *et al.* Phylogeny and origins of hantaviruses harbored by bats, insectivores, and rodents. *PLoS Pathog* 2013;9:e1003159.
8. Shi M, Lin XD, Chen X, Tian JH, Chen LJ *et al.* The evolutionary history of vertebrate RNA viruses. *Nature* 2018;556:197–202.
9. Plyusnin A, Morzunov SP. *Virus Evolution and Genetic Diversity of Hantaviruses and Their Rodent Hosts*. Berlin, Heidelberg: Springer. pp. 47–75.
10. Rowe JE, Wagoner K, Jentes ES, Root JJ, Beaty BJ *et al.* Epizootiology of Sin Nombre and El Moro canyon hantavirus, southeastern Colorado, 1995-2000. *J Wildl Dis* 2013;41:1–11.
11. Kallio ER, Voutilainen L, Vapalahti O, Vaheri A, Henttonen H *et al.* Endemic hantavirus infection impairs the winter survival of its rodent host. *Ecology* 2007;88:1911–1916.
12. Kallio ER, Klingström J, Gustafsson E, Manni T, Vaheri A *et al.* Prolonged survival of Puumala hantavirus outside the host: evidence for indirect transmission via the environment. *J Gen Virol* 2006;87:2127–2134.
13. Botten J, Mirowsky K, Kusewitt D, Ye C, Gottlieb K *et al.* Persistent Sin Nombre virus infection in the deer mouse (*Peromyscus maniculatus*) model: sites of replication and strand-specific expression. *J Virol* 2003;77:1540–1550.
14. Miedema K, Schountz T, McGuire A, Fauver J, Rico A *et al.* Maporal hantavirus causes mild pathology in deer mice (*Peromyscus maniculatus*). *Viruses* 2016;8:286.
15. Martinez-Valdebenito C, Calvo M, Vial C, Mansilla R, Marco C *et al.* Person-to-person household and nosocomial transmission of Andes hantavirus, southern Chile, 2011. *Emerg Infect Dis* 2014;20:1637–1644.
16. Brummer-Korvenkontio M, Vaheri A, Hovi T, von Bonsdorff CH, Vuorimies J *et al.* Nephropathia epidemica: detection of antigen in bank voles and serologic diagnosis of human infection. *J Infect Dis* 1980;141:131–134.

17. Feldmann H, Sanchez A, Morzunov S, Spiropoulou CF, Rollin PE *et al.* Utilization of autopsy RNA for the synthesis of the nucleocapsid antigen of a newly recognized virus associated with hantavirus pulmonary syndrome. *Virus Res* 1993;30:351–367.
18. Cosgriff TM. Mechanisms of disease in hantavirus infection: pathophysiology of hemorrhagic fever with renal syndrome. *Clin Infect Dis* 1991;13:97–107.
19. Meyer BJ, Schmaljohn CS. Persistent hantavirus infections: characteristics and mechanisms. *Trends Microbiol* 2000;8:61–67.
20. Vapalahti O, Lundkvist A, Kukkonen SK, Cheng Y, Gilljam M *et al.* Isolation and characterization of Tula virus, a distinct serotype in the genus hantavirus, family Bunyaviridae. *J Gen Virol* 1996;77:3063–3067.
21. Jääskeläinen KM, Plyusnina A, Lundkvist A, Vaheri A, Plyusnin A. Tula hantavirus isolate with the full-length ORF for non-structural protein NSS survives for more consequent passages in interferoncompetent cells than the isolate having truncated NSS ORF. *Virology* 2008;5:3.
22. Elmore S. Apoptosis: a review of programmed cell death. *Toxicol Pathol* 2007;35:495–516.
23. Li X-D, Mäkelä TP, Guo D, Soliymani R, Koistinen V *et al.* Hantavirus nucleocapsid protein interacts with the Fas-mediated apoptosis enhancer Daxx. *J Gen Virol* 2002;83:759–766.

Fig 1.

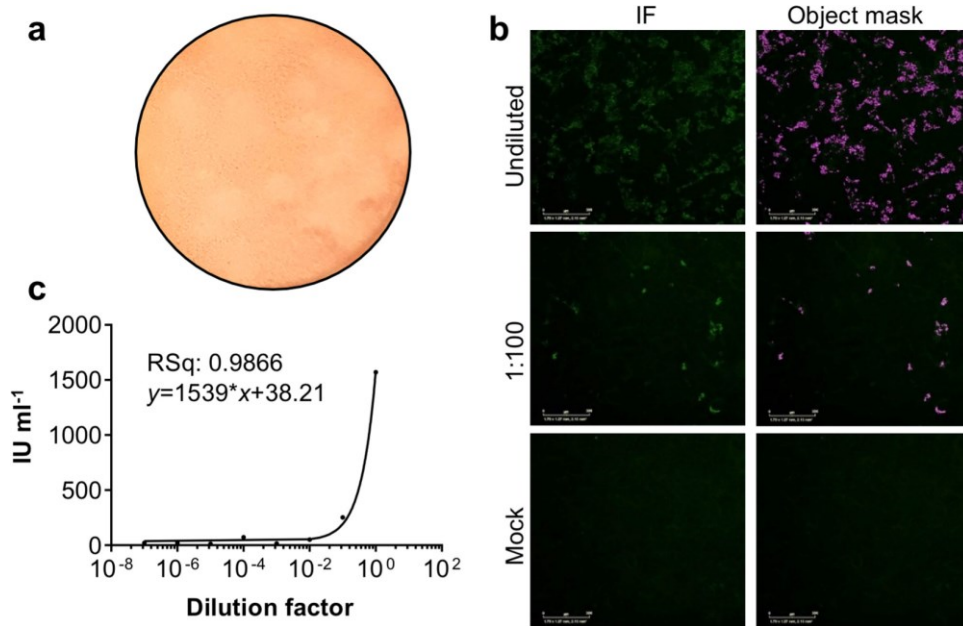


Fig 2.

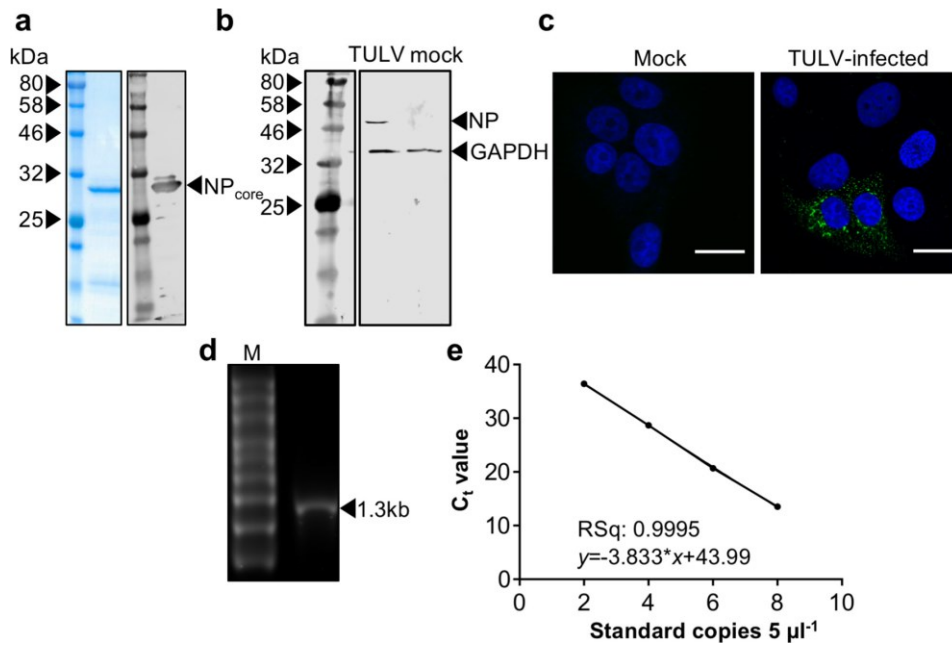


Fig 3.

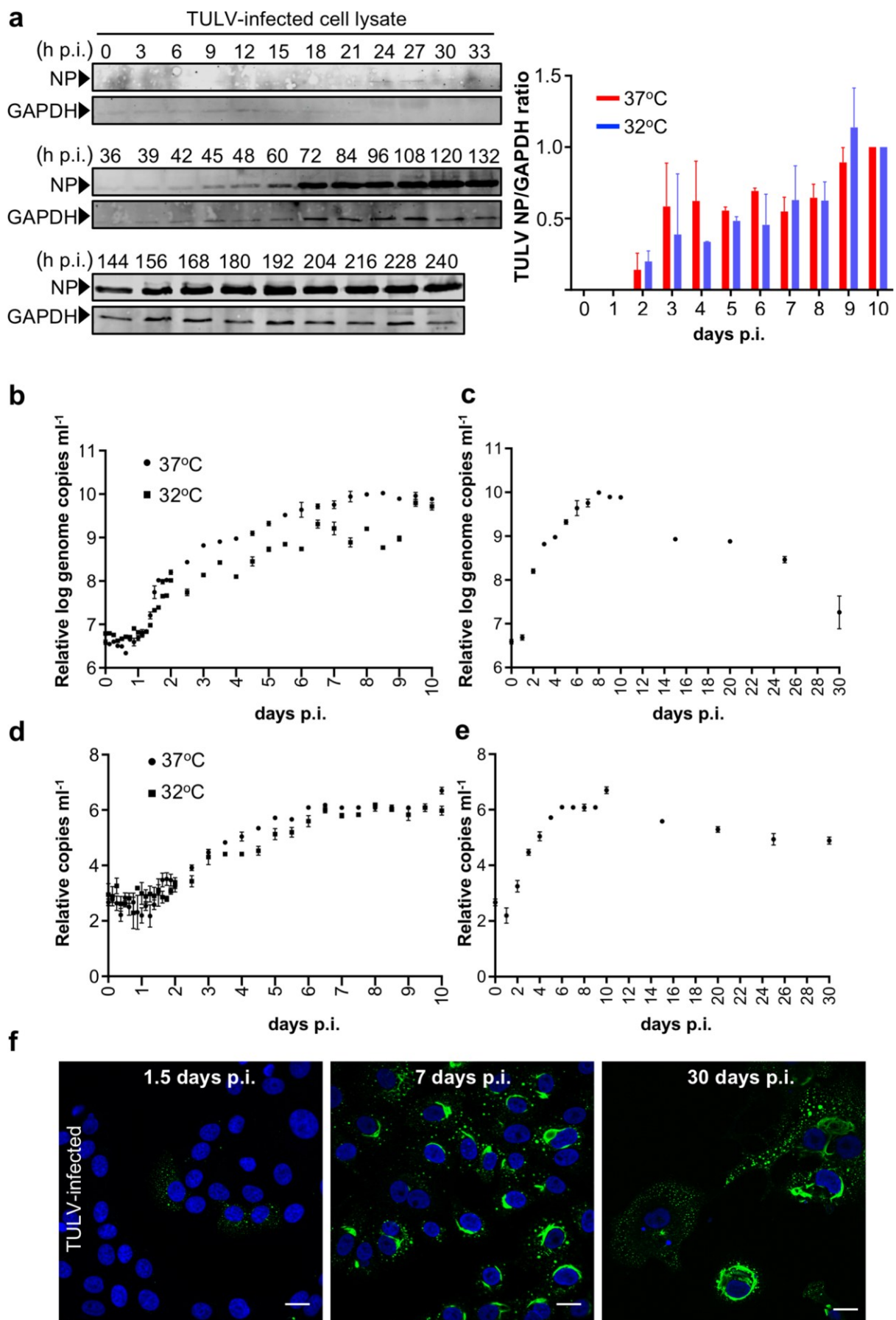


Fig 4.

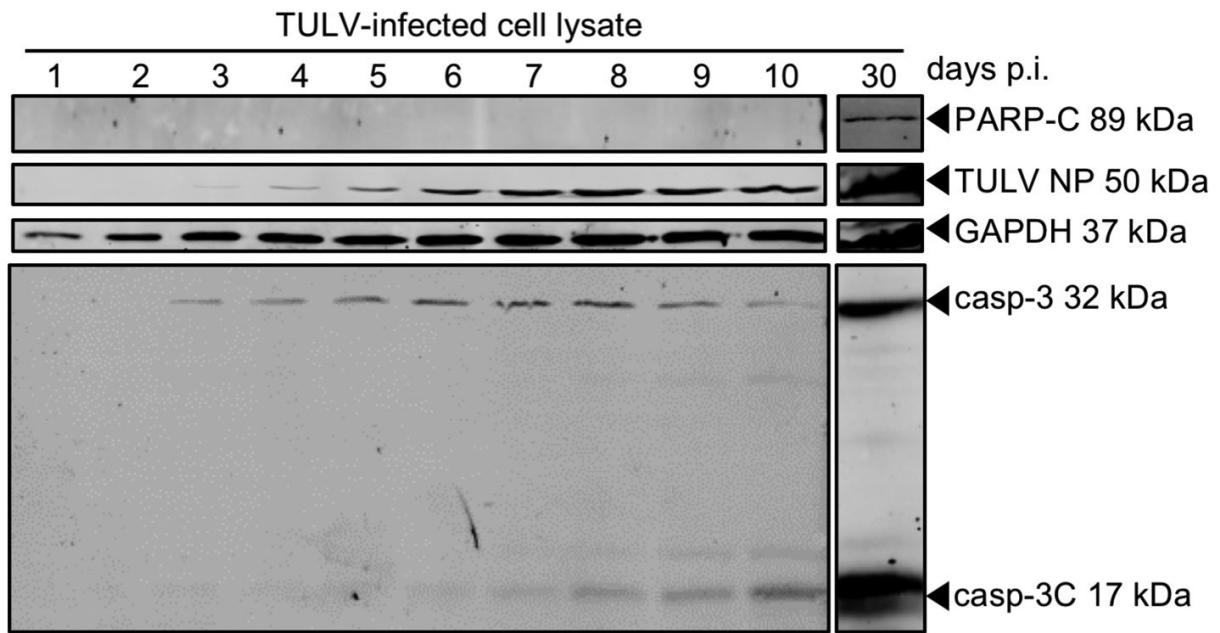


Fig 5.

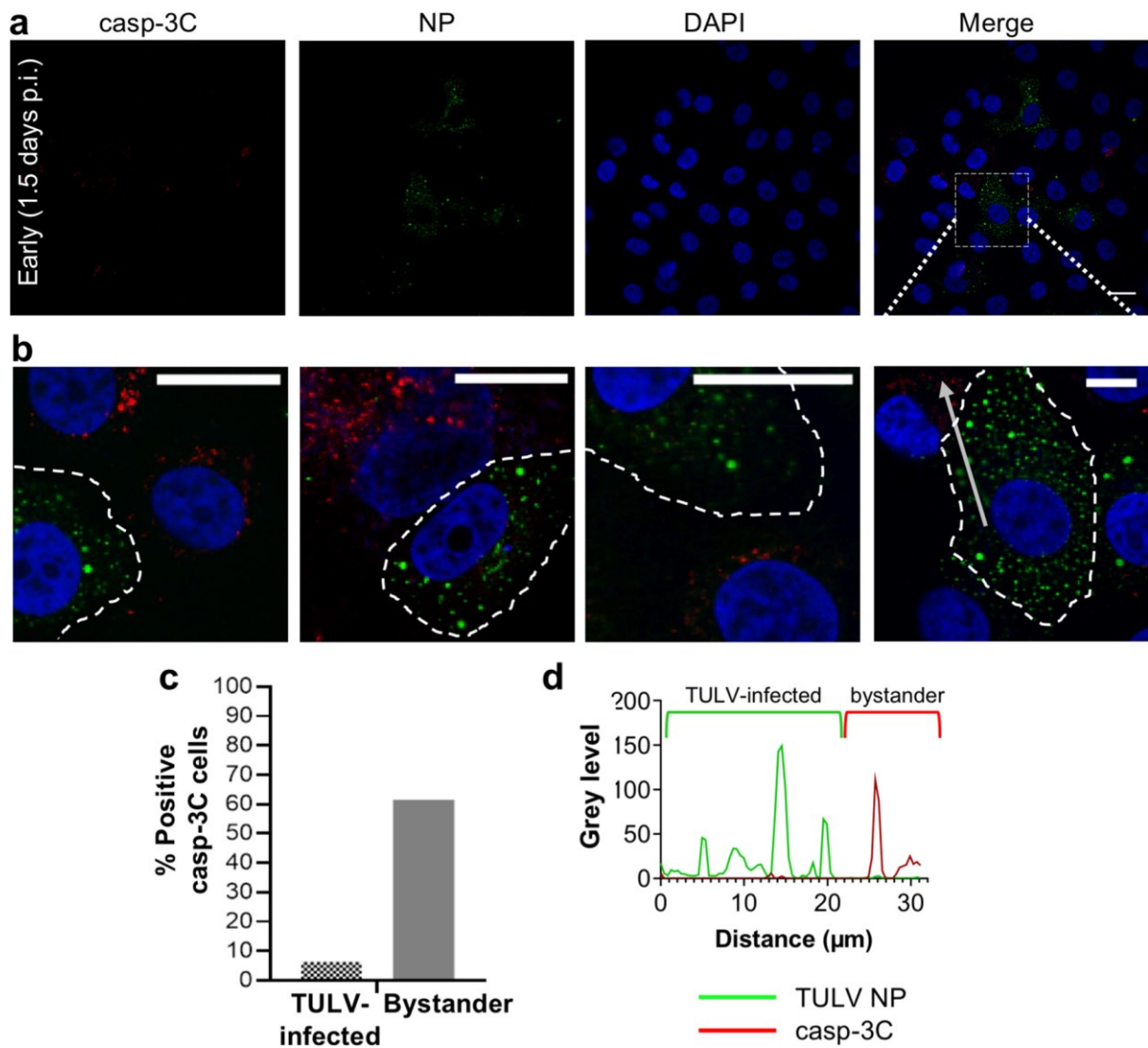


Fig 6.

